J Surg Res 2022; 5 (1): 115-133 *DOI: 10.26502/jsr.10020206*

Research Article

Contribution of Statistical Iterative Reconstruction Algorithm for Orthopaedic Applications: A Study with a Cone-Beam CT Prototype

Stéphanie UK[1], Fanny Morin[2], Valérie Bousson[3], Rémy Nizard[4], Guillaume Bernard[2], Christine Chappard[*1]

[1]B3OA, UMR CNRS 7052, Inserm U1271 Université de Paris, 10 avenue de Verdun, 75010 Paris, France

[2]THALES AVS, 460 rue du Pommarin, 38430 Moirans, France

[3]Service d'Imagerie Ostéo-Articulaire, Viscérale et Vasculaire, Hôpital Lariboisière, APHP, Nord Université de Paris, 2 rue Ambroise Paré, 75010 Paris, France

[4]Département d'Orthopédie Hôpital Lariboisière, 2 rue Ambroise Paré, 75010 Paris, France

[*]**Corresponding author:** Christine Chappard, MD, PhD. B3OA, UMR CNRS 7052, Inserm U1271 Université de Paris, 10 avenue de Verdun, 75010 Paris, France

Received: 08 November 2021; **Accepted:** 15 November 2021; **Published:** 14 March 2022

Citation: Stéphanie UK, Fanny Morin, Valérie Bousson, Rémy Nizard, Guillaume Bernard, Christine Chappard. Contribution of Statistical Iterative Reconstruction Algorithm for Orthopaedic Applications: A Study with a Cone-Beam CT Prototype. Journal of Surgery and Research 5 (2022): 115-133.

Abstract

Three-dimensional reconstruction for image-guidance in orthopaedic surgery necessitates a high degree of geometrical precision but not necessary structure details. With the aim to reduce as much as possible the dose, a cone beam CT prototype was tested with decreasing intensities, the number of projections or different angular range. We tested two methods of reconstruction: Feldkamp-Davis-Kress (FDK) reconstruction and the Simultaneous Algebraic Reconstruction Technic with Total Variation (SART-TV). Based on this protocol, on a knee cadaveric specimen, we combined qualitative assessment performed by radiologists and orthopedic surgeons, objective metrics of image quality such as signal-to-noise ratio, or related to bone geometric contour, grey level restitution and texture of trabecular bone, and finally the quality of joint space segmentation. Objective indicators related to signal-to-noise ratio, the quality of geometry and segmentation have shown better results for SART-TV than FDK in case of

decrease projections number and angular range. On the contrary, qualitative assessment, and indexes about grey level restitution and textural quality of trabecular bone produced the best results for FDK reconstruction. These results showed that SART-TV reconstruction has a good capability to restore the geometry in case of low dose protocol and consequently could be a good candidate for orthopaedic surgery.

Key Words: Cone beam computed tomography; Image processing; Computer assisted; Dosimetry radiation; Orthopaedic surgery; Bone

Abbreviations

ART: algebraic reconstruction technique, CB-CT: cone beam-computed tomography, CT: computed tomography, DAR: decreasing angular range, DAS: decreasing angle subsample, DiffEntropy: Difference Entropy, ENT: entropy, FBP: filtered back-projection, FDK: Feldkamp, David and Kress, FOV: field of view, IR: iterative reconstruction, MRI: Magnetic Resonance Imaging, RMSE: Root Mean Square Error, SART: Simultaneous Algebraic Reconstruction Technic, SIRT: simultaneous iterative reconstruction technique, TV: Total Variation, SNR: Signal to Noise Ratio, SSMI: Structure Similarity Index.

1. Introduction

Fluoroscopic C-Arms are widely used in operating rooms first for qualitative assessment and to obtain visual references for guiding tools in orthopaedic surgery and interventional radiology. Images classically obtained with a C-Arm are 2D projections according to different orientations. Increasingly C-arms are being equipped with flat panel detectors, which provide significant contrast and spatial resolution improvement over image intensifier detectors [1]. 3D reconstruction for advanced image guidance during orthopaedic or radiologic interventions can be obtained with C-arms projections but requires a high degree of geometrical precision, fast acquisition time, and large field of view to encompass the observed anatomical structures [2]. The combination of a conical X-ray beam with a flat panel detector defines cone-beam CT (CB-CT): the conical X-ray beam covers a large volume with a single rotation acquisition. The Z coverage afforded by this CT is large enough to image an entire organ in one axial scan [3]. The classical reconstruction method used is the Feldkamp, David and Kress (FDK) algorithm, which is an adaptation of filtered back-projection (FBP) reconstruction for cone-beam acquisition [4]. This method is mainly used for images in the dental and maxillo-facial surgery fields [5]. However, in orthopaedic surgery, there is a need for wider flat-panel detectors. For instance, few experiments have been performed in acute spine trauma surgery [6], in pedicle screw placements [7], to correct axial malrotation of the femoral shaft after fracture [8], or for tibial plateau fracture reduction [9]. Unlike conventional CT, for which 360° rotation gantry is necessary, C-arm devices typically use a 200° rotation (180°+ fan beam angle) [10]. One can then reconstruct a 3D volume from 2D projections with sub-millimeter 3D spatial resolution and with isotropic voxels [2,3,11]. The main advantage of CB-CT is that the radiation dose is much smaller than with conventional CT because of differences in imaging geometry and collimation of X-rays [10,12]. Other advantages of CB-CT are the low cost and the high compactness and portability as compared with other technologies [13]. However, there are also few disadvantages: scattered radiation, relatively limited dynamic range of x-ray detectors, potential truncated

views and beam hardening artifacts [14]. Moreover, the limitation of the angular span poses a great challenge in image reconstruction. These drawbacks can affect the quality of images and potentially any segmentation process. The usual strategy to reduce the radiation exposure for both patients and staff is to decrease the voltage or current, but another strategy in conventional CT could be to use iterative reconstruction (IR) methods with fewer projections, which is an alternative to FBP [15]. There are multiple algebraic methods using iterative methods, with three main families: projective methods, a statistical method for noise reduction, and finally compressed sensing reduction of projection number. The adaptative statistical IR method has been found reliable to reduce the dose, with acceptable image quality despite low tube intensity [16,17]. The oldest method is the projective one based on a ray-by-ray method passing pixels by pixels called the algebraic reconstruction technique (ART), resulting volumes might be quite noisy, but the convergence rate is high (i.e., few iterations needed) [18]. The simultaneous IR technique treats all rays at the same time (i.e., all pixels of all projections). There is less noise in reconstructions, but the algorithm requires more iterations to converge [19]. Simultaneous ART (SART) is a hybrid of ART and simultaneous IR technique and is compatible with a clinical acquisition time with little noise and a good convergence rate [20]. This method was previously tested for 3D cone-beam reconstruction [19]. It treats the ray projection by projection, sampling is based on a group of voxels including potentially sub-volume voxels. In addition, SART proposes to add a Hann window during projection. Finally, ordered-subset SART is based on SART, but projections are not treated independently but rather subset by subset. As previously, less noise is observed in reconstructed volume but at higher convergence cost [19]. To improve the quality for clinical requirements, Total variation (TV) based regularization method was able to suppress streak like artifacts for few CT [21]. The goal of our study was to test the performance in terms of image quality of a CB-CT prototype evaluated under different imaging conditions for orthopaedic surgery application. We compared 3D image reconstructions obtained with the CB-CT prototype at different tube currents, with different numbers of projections and angular span and with FDK or an IR method, specifically SART-TV.

2. Materials and methods

2.1 Experimental setup

The CB-CT prototype was equipped with a detector Thales Pixium (2630S); the source-detector distance was 122 cm, object–detector distance 15 cm providing a 2000*2000 mm volumetric field of view (FOV), and pixel size of the detector 260 µm (matrix size: 768x768). The spot size of the x-ray source was 0.6 mm with 15° divergence and was operated in pulsed mode. The tube potential was fixed at 70 kVp; the effective tube currents tested were 15, 10 and 5 mA with exposure time 20 ms. An aluminum filter of 2 mm was applied in addition to the 2.5-mm (equivalent Al) inherent filter. The motor rotates in an orbital range of 360° collecting 720 projections with a total duration scan of 1 min. The projections were corrected for offset, gain and defects only, and a geometric calibration provided projection matrices to capture the source-detector position and orientation of each acquisition. At 70kVp with 360° and 20 ms per acquisition, the dose measurement was directly performed on the detector (R 225 ACS Ralco). The absorbed dose was 0.5 mGy at 5 mA, 0.8 mGy at 10 mA and 1.2 mGy at 15 mA.

2.2 Specimen and imaging acquisition

One knee specimen from the Institute of Anatomy, Paris Descartes University, was used. The subjects willed their body to science and were anonymous. The study was approved by the Ethics Committee of Paris University, Paris. The Tissues collection was approved by Direction Générale de la Recherche et de l'Innovation-Cellule Bioéthique (n°DC-2018-3366). The collection of these human tissue specimens was performed in accordance with their guidelines and regulation. Because of this regulation, no data were available regarding the cause of death, previous illnesses, or medical treatments of this individual. After soft-tissue removal, the knee specimen was stored at −20°C, then scanned in an upright position.

2.3 Image reconstruction

In the first scenario, decreasing angular subsample (DAS), the number of projections was reduced from 400 to 80, with a reduction of 40 projections for each reconstruction, but a fixed angular range at 200°. In the second scenario, decreasing angular range (DAR), both the number of projections and angular range were reduced in parallel, from 200° to 140°, with number of projections ranging from 200 to 140. These two scenarios were tested with three different currents: 15, 10, and 5mA (Figure 1A).

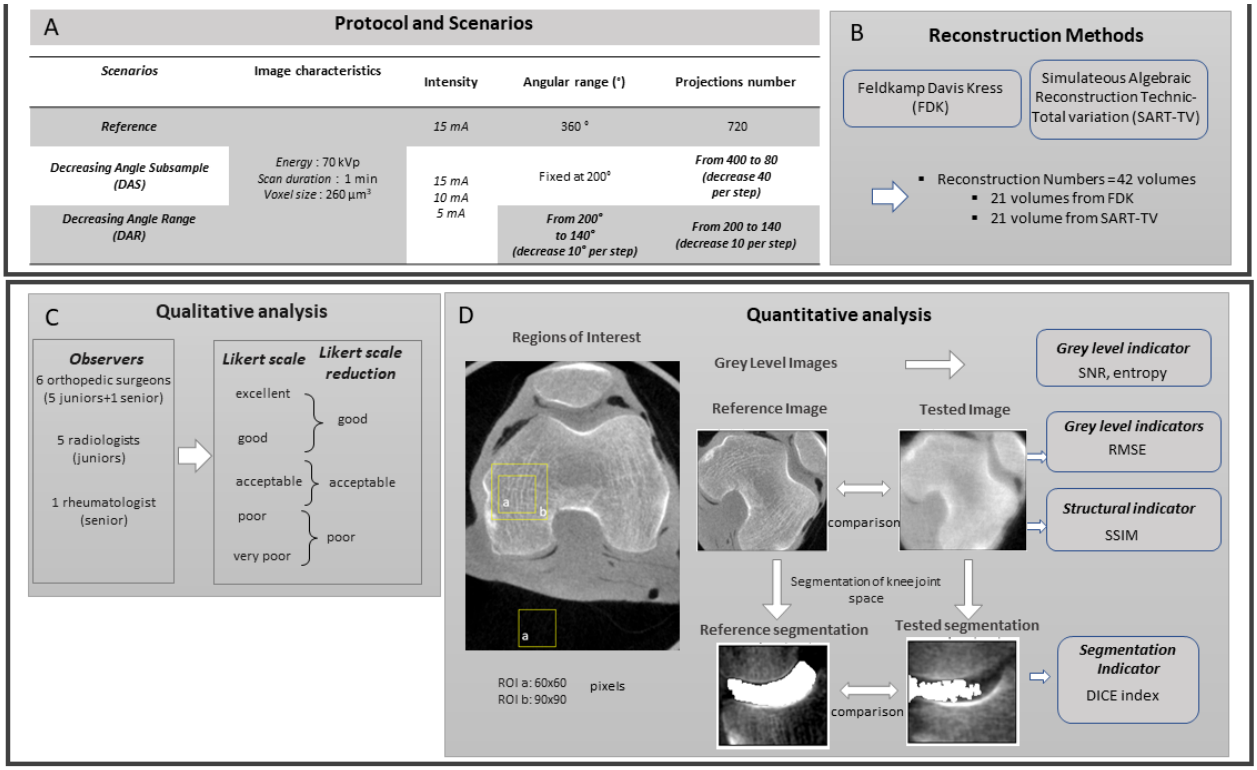

Figure 1: Description of the protocol performed on one knee specimen, acquisition and different scenarios of reconstruction (A), reconstruction methods with the number of volume reconstructs (B), qualitative analysis (C) and quantitative analysis (D).

Analytical reconstruction methods such as FBP have been adapted considering conical acquisition geometry and were developed by Feldkamp, Davis and Kress in 1984 [4]. The FDK algorithm is based on three main steps. First, a cosine weight is applied to the projections. Then, the projections are filtered in the frequency domain using a ramp filter combined with a Hann window. Finally, the filtered projections are back-projected to reconstruct the volume (Figure 1B). The state of the art for the algebraic method, the ART, is based on projective method developed by G. Herman and coworkers, it seeks to minimize the "alpha" value, the approximate value reducing the distance between P and [A] [18]. Alpha is calculated by the least square method:

$$J(\alpha) = \|P - [A].\alpha\|^2 \qquad (1)$$

where α is the operator matrix projection, all projective methods look for the alpha value to minimize J(α), a convex function, which is noted by:

$$\alpha = argmin J(\alpha) \qquad (2)$$

We used SART-TV, projections were ordered to optimize entropy between two consecutive projections as the subset size was set to 1 projection (i.e., one angle at once) (Figure 1B) [20]. The convergence is calculated by measuring the differences between two iterations in the images, in our case 4 iterations have been necessary. To improve image quality and reduce noise with a good convergence rate, the convergence does not take place toward a point but toward a zone and the zone depends on the starting point. Moreover, TV regularization was added to increase image quality in case of sparse acquisitions [21]. Image reconstructions in 16 bits obtained with the two reconstruction methods (FDK and SART-TV) for the different scenarios showed variable quality of images (Figure 2).

2.4 Segmentation method

We previously developed a semi-automatic segmentation method of the joint space on CT images [22]. Briefly, the method is applied on the frontal view, and a region of interest corresponding to the medial compartment of the knee is manually selected. For removing noise, a circular averaging filter within the square matrix of 8 size is used. For extracting bone from soft tissues, a hysteresis threshold method using the quantile of grayscale followed by morphological operations (closing and opening operators) is used. Finally, the user draws 15 control points in the pertinent region for initializing the snake model. The process involves using MATLAB. We compared the segmentation results between the referent reconstructions and the different scenarios.

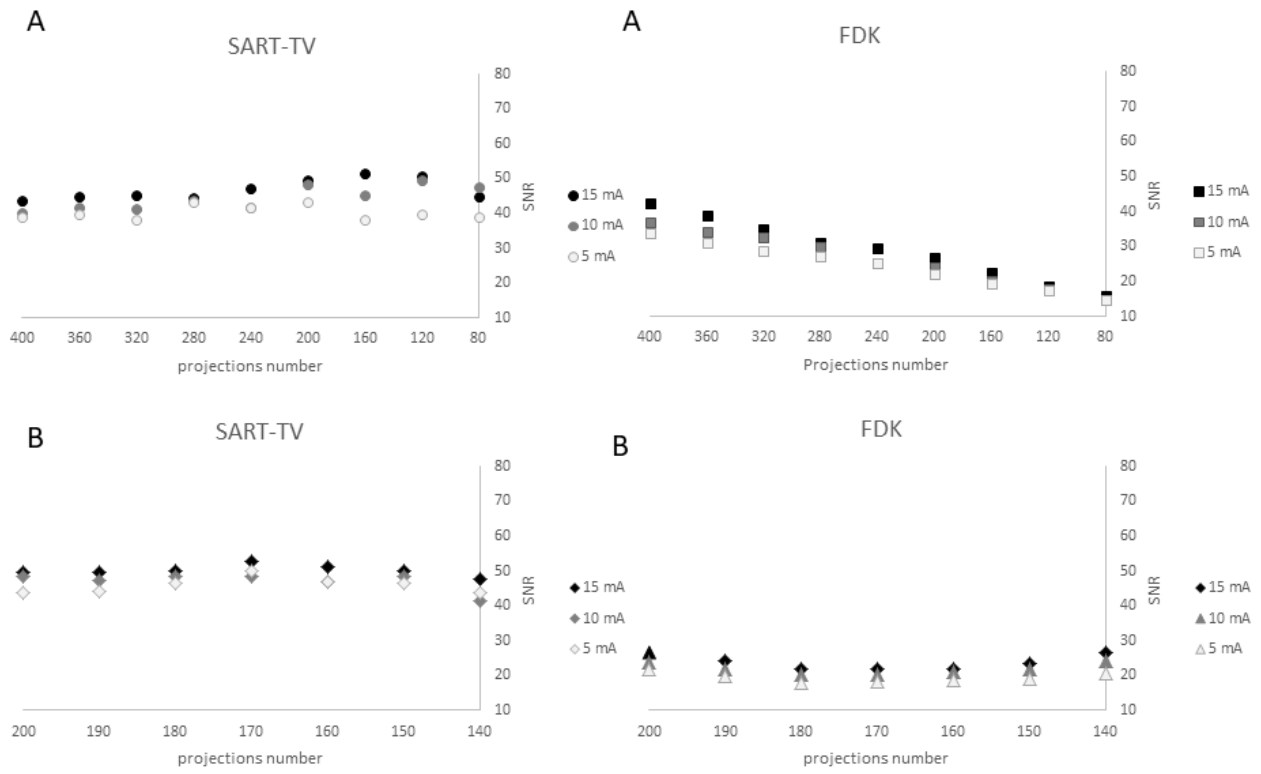

Figure 2: Signal-to-noise ratio (SNR) according to projection number with fixed angular range of acquisition, 200°, and various projection numbers (decreasing angular subsample scenario) for the two methods of reconstruction: SART-TV (A) and FDK (A).

SNR according to the projection number with variable angular range of acquisitions from 200°to 140° with equivalent number of projections (decreasing angular range scenario) reconstructed with the two methods: SART-TV (B) and FDK (B).

2.5 Image quality analysis

Frontal and transverse views of the reconstructions were selected from the three situations mentioned above. Finally, we randomly displayed 90 anonymized images: 6 reference images (720 projections, 360°) performed at different currents: 15, 10, and 5 mA with the 2 methods of reconstruction, FDK and SART-TV, for 42 images with decreasing number of projections and fixed 200° rotation angle (scenario DAS) and 42 images with decreasing number of projections and rotation angle 200° to 140° (scenario DAR). In total, 12 physicians- 6 orthopedic surgeons (5 junior resident and 1 senior surgeon with an experience of 20 years) and 5 junior radiologist residents and 1 rheumatologist with an experience of 20 years in quantitative analysis in osteo-articular diseases and bone imaging- scored images with blinding by using a Likert scale from 1, very poor; 2, poor; 3, acceptable; 4, good; 5, excellent. Finally, to simplify analyses, poor and very poor were pooled, as were good and excellent (Figure 1C). For

quantitative analysis, we used five indicators depending on grey level that described the quality of contours and segmentation quality (Figure 1D). We evaluated the signal-to-noise ratio (SNR), the ratio between the mean gray scale of bone *(MeanBone)* and the standard deviation of air around *(StDvAir)* in a region of interest (60x60 pixels). The positioning of the ROI is displayed on Figure 1D.

$$SNR = \frac{MeanBone}{StDvAir} \quad (3)$$

For all other quality indicators, the FDK reconstruction with complete 360° rotation and 720 projections at 15 mA was the reference compared to the different scenarios (Figure 1D). For evaluating texture, we calculated the entropy (ENT) in a region of interest in bone of 90x90 pixels (Figure 1D). The higher the entropy, the coarser the granulation of the image is. We used the following formula:

$$ENT = \sum_i \sum_j P(i,j) \log P(i,j) \quad (4)$$

where *P(i,j)* corresponds to element of co-occurrence matrix. We calculated the difference entropy *(DiffEntropy)* as the absolute value of the difference between the reference image and tested images [23].

The root means square error (RMSE) of the gray value images was calculated according to the Gonzalez definition [24]. The images reconstructed with the SART-TV and FDK reconstructions according to the different scenarios were compared to the reference volume obtained with FDK reconstruction with complete 360° rotation and 720 projections at 15 mA.

$$RMSE = \sqrt{\frac{1}{n_x n_y} \sum_0^{n_x-1} \sum_0^{n_y-1} [imgR(x,y) - imgD(x,y)]^2} \quad (5)$$

where *imgR* is the reference image and *imgD* the tested image. Then we used the structural similarity index (SSIM) plugin developed by Renieblas et al. and defined in the following formula [25]:

$$SSIM(x,y) = \frac{(2\mu_{ImgR}\mu_{ImgD}+C_1)(2\sigma_{ImgR}\sigma_{ImgD}+C_2)}{(\mu_{ImgR}^2+\mu_{ImgD}^2+C_1)(\sigma_{ImgR}^2+\sigma_{ImgD}^2+C_2)} \quad (6)$$

The small constants *C1, C2* stabilize the computation of the equations when denominators become small with $C1 = (0.01*L)^2$ and $C2=(0.03*L)^2$ where L is the grey level number of the image therefore 65025. These methods assessing perceptual image quality allowed for quantifying errors between a distorted image and the reference image. SSIM gives edge information between the reference and test images [25]. These two metrics are classically used to assess model performance [26]. To evaluate segmentation results of the knee joint space from the frontal central image, similarity coefficient index DICE values were calculated, with the coefficient defined as follows:

$$DICE\left(Seg_{Ref}, Seg_{Deg}\right) = \frac{2\left(Seg_{Ref} \cap Seg_{Deg}\right)}{\left(Seg_{Ref} + Seg_{Deg}\right)} \quad (7)$$

where Seg_{Ref} is the JS segmentation from the reference image considered as ground truth and Seg_{Deg} is the JS segmentation from the tested images. The DICE values range from 0 to 1; DICE = 1 means complete overlap; DICE 0–1, partial overlap; and DICE = 0, no overlap. A DICE value > 0.7 has been reported as good similarity performance [27].

3. Results

The description of the protocol performed on one knee specimen, acquisition and different scenarios of reconstruction is shown in the Figure 1. As a

benchmark, the FDK reconstruction was performed with large number of views: 720 projections over 360° at 15 mA. In the number of projections reduction scenario (DAS scenario: 400 to 80 decreasing projections, fixed 200° angle), with SART-TV reconstruction, mean signal-to-noise ratio (SNR) was 43.9 (range 38.4 to 51.6) and was relatively constant for number of projections > 280; the results were slightly better at 15 than 10 and 5 mA (Figure 2). With FDK reconstruction, SNR values regularly decreased from 42.2 to 14.5 with decreasing number of projections from 400 to 80. In the decreasing angular range scenario (DAR scenario: from 200° to 140° with one projection every degree), with SART-TV, the mean SNR was 47.6 (relatively constant from 41.4 to 52.7); with FDK, the mean SNR was lower, 21.7 (relatively constant from 17.9 to 26.6) (Figure 2). In the DAS scenario, the Difference of the textural parameter Entropy measured in a trabecular bone region of interest between reference images and tested images was higher with SART-TV than FDK, with an increase that appeared with < 200 projections, the results were paralleled in the DAR scenario (Figure 3). The qualitative grading based on a Likert scale was clearly biphasic with SART-TV after 200 projections; we found a clear drop-off in quality assessment as a function of projection number (Figure 4). Indeed, with < 200 projections, no image was identified to have a good quality. The situation was less obvious with FDK, for which the quality was more frequently qualified as good (Figure 4). The Root Mean Square Error (RMSE) results increased with SART-TV from 400 to 80 projections and especially < 200 projections and was constantly higher with 5 mA than 15 or 10 mA (Figure 4). The behavior was similar with FDK but with less discrepancy between 400 to 80 projections and no differences between 15, 10 and 5 mA (Figure 4). The RMSE results from 200 to 140 projections with reduction in angular range were higher at 5 than 10 and 15 mA, with a deep increase at < 180 to 170 projections with SART-TV and a similar pattern with FDK (Figure 5). The Structural Similarity Index (SSIM) with FDK was systematically less than with SART-TV for both DAS and DAR scenarios (Figure 6). The SSIM difference between SART-TV (circle) and FDK (square) was about 4.6% for 15 and 10 mA and about 7% for 5 mA until 200 projections. With 160 and 120 projections, the difference was about 12.5% at both 15 and 10 mA and 17.1% at 5 mA and was 22.8% for 80 projections at 15 and 10 mA and 26.4% at 5 mA. For the DAR scenario, with reduction of angular range, the SSIM was systemically less with FDK (triangle) than SART-TV (diamonds). The mean difference was 4.5% at 15 mA, 5.2% at 10 mA and 8.7% at 5 mA. With the DAS scenario and SART-TV, the mean DICE similarity coefficient was 0.82 (range 0.72 to 0.94) and with FDK, 0.64 (range 0.13 to 0.94) (Figure 7). With the DAR scenario, the mean DICE coefficient was 0.94 (range 0.72 to 0.94) with SART-TV and 0.64 (range 0.13 to 0.94) with FDK. DICE values > 0.7 indicate good similarity with the reference. Whatever the number of projections, SART-TV gave relatively stable results with slightly better DICE values at 15 mA. In contrast, with FDK, results were dissipated and less coherent between different projections whatever the intensity. With the DAR scenario, DICE values ranged from 0.59 to 0.96 with SART-TV and 0.13 to 0.95 with FDK, with large discrepancies not depending on the intensity. As a conclusion, the segmentation was more efficient with SART-TV than FDK reconstruction and especially in the DAS scenario.

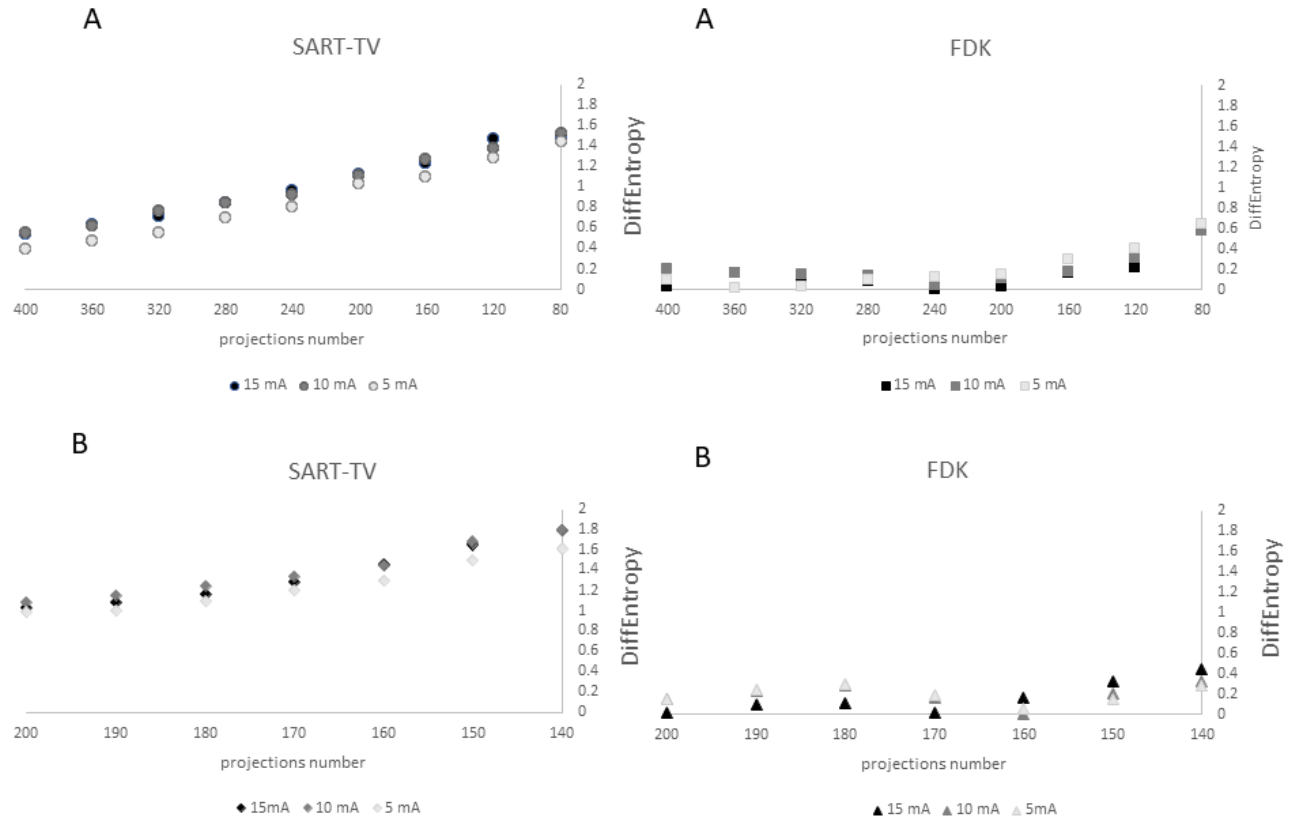

Figure 3: Differences in entropy compared to the reference image (15 mA, 360°, 720 projections) in a region of interest inside bone according to the projection number with a fixed angular range of acquisition: 200° and various projection numbers (scenario decreasing angular subsample) for the two methods of reconstruction: SART-TV (A) and FDK (A).

Differences in entropy compared to the reference image (15 mA, 360°, 720 projections) in a region of interest inside bone according to the projection number with an angular range of acquisition from 200° to 140° and the same number of projections for the two methods of reconstruction: SART-TV (B) and FDK (B).

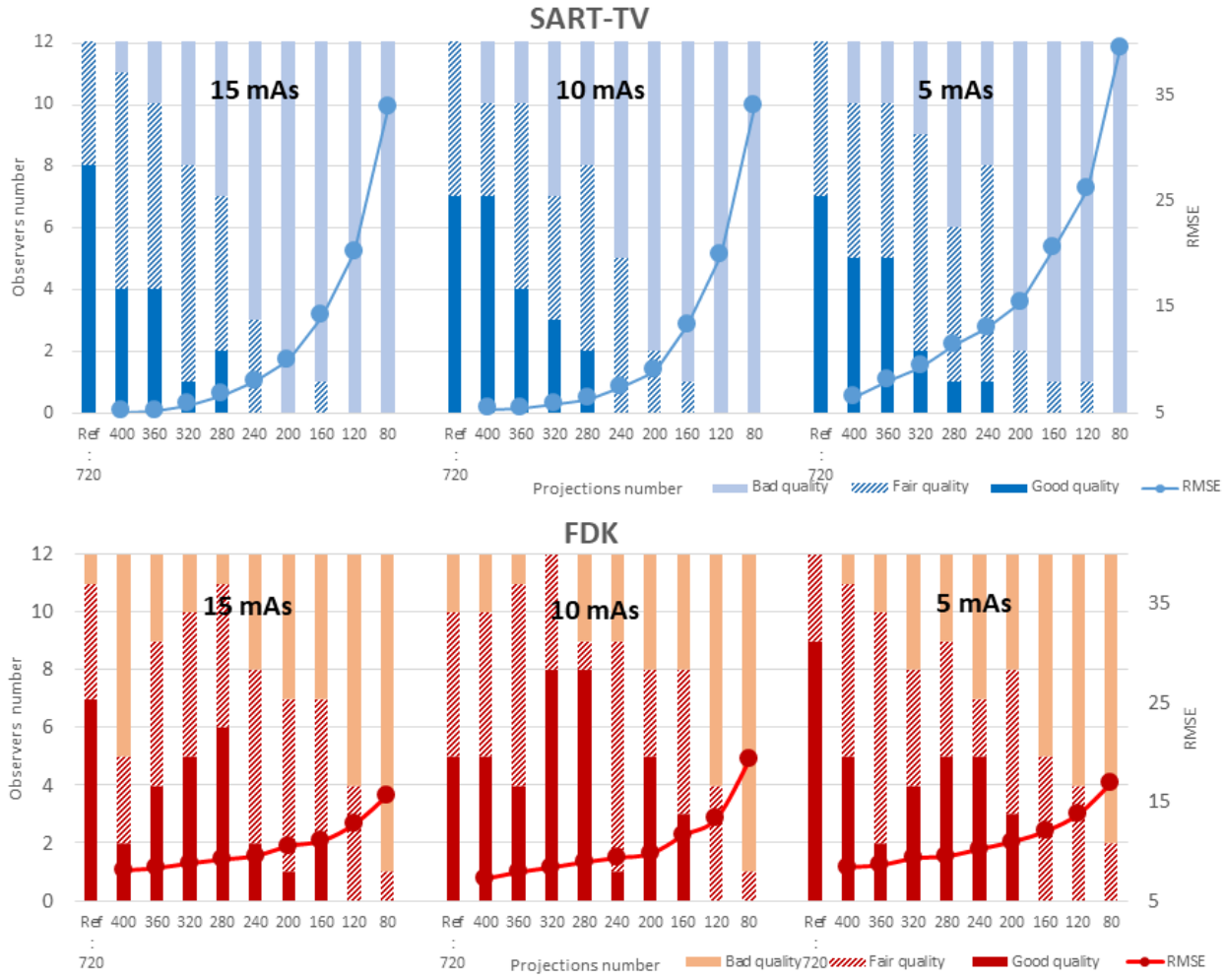

Figure 4: Qualitative analysis and root mean square error (RMSE) values with decreasing number of projections and a fixed angular rotation of 200° with 3 different currents, 15, 10 and 5 mA, for the two methods of reconstruction: SART-TV and FDK. The right abscissa is the number of observers and the left is the RMSE.

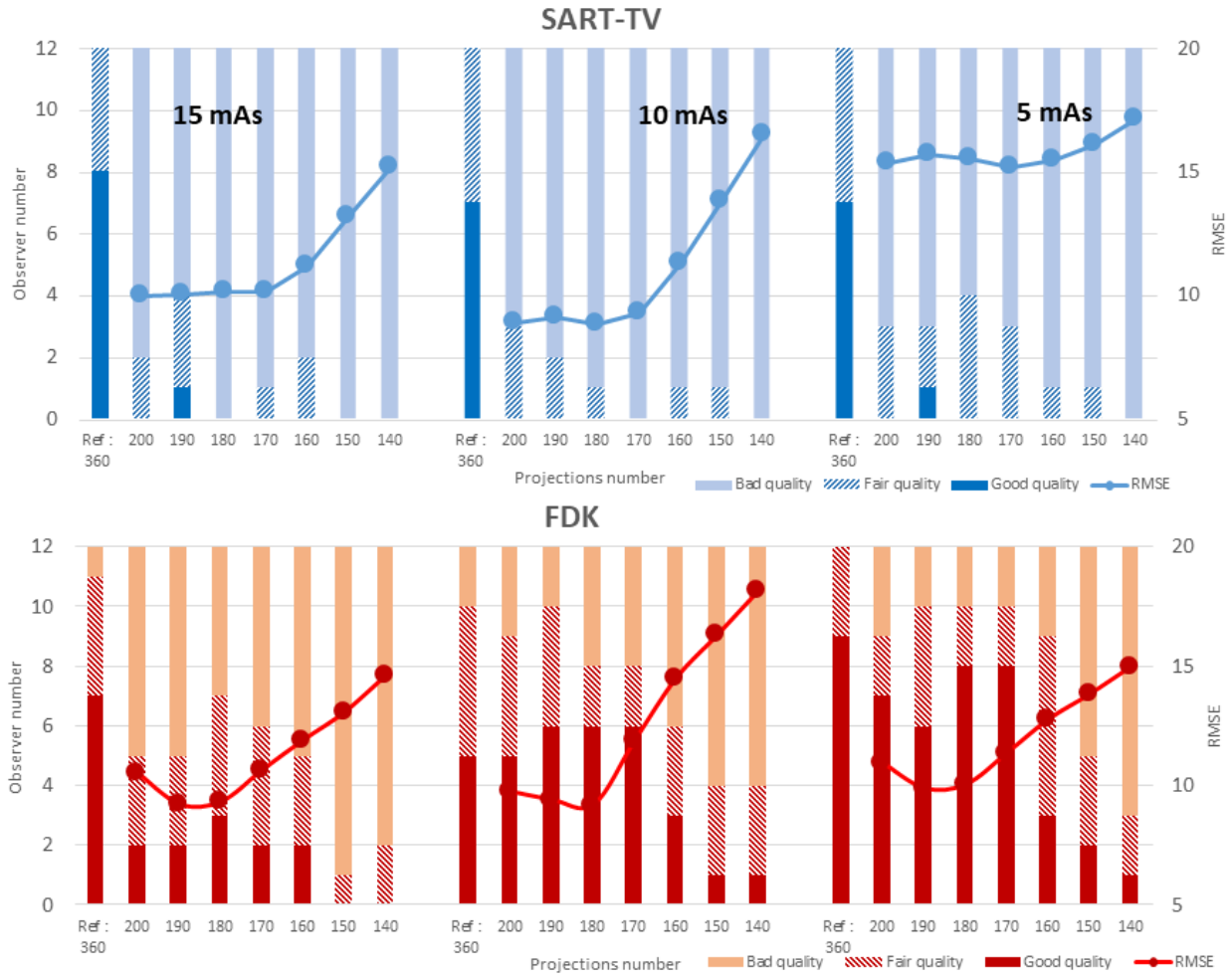

Figure 5: Qualitative analysis and RMSE values with decreasing number of projections and decreasing angular range from 200° to 140° with 3 currents, 15, 10 and 5 mA, for the two methods of reconstruction: SART-TV and FDK. The right abscissa is the number of observers and the left is the Structural Similarity Index (SSIM) value varying from 1 to 0 (1 is perfect similarity and 0 absence of similarity).

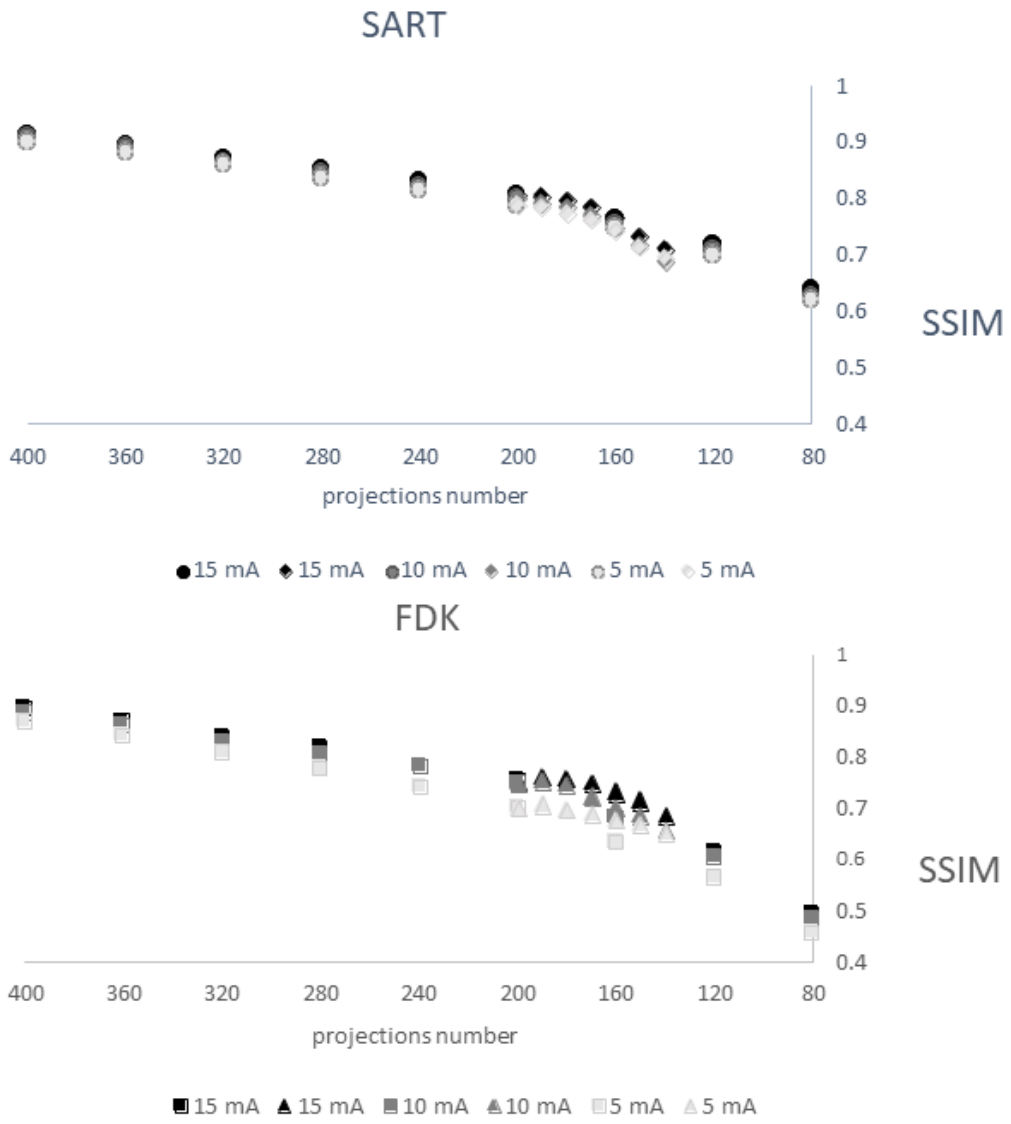

Figure 6: SSIM values according to projection number with fixed angular range of acquisition, 200°, and projection number from 400 to 80 (decrease number of projections, circles) and from 200° to 140° (decrease angular range, lozenges) for the two methods of reconstruction: SART-TV and FDK.

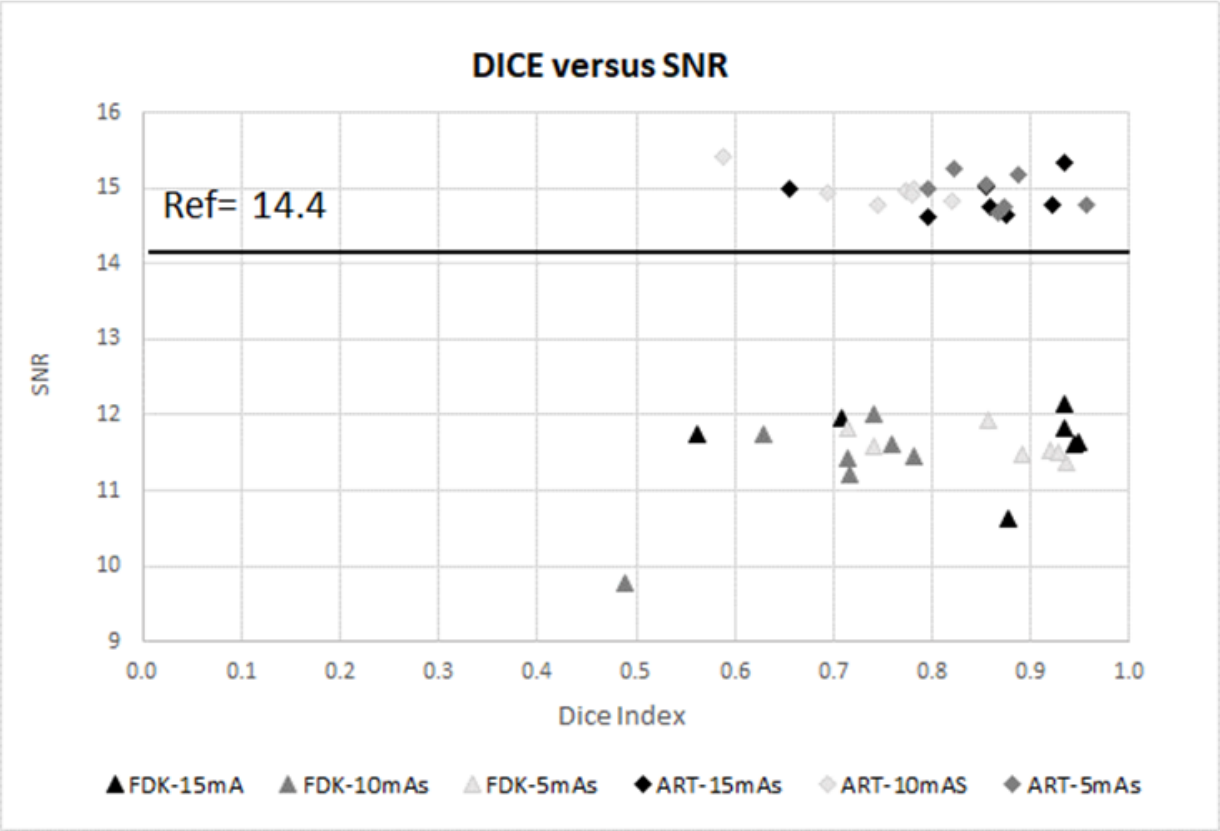

Figure 7: Distribution of DICE results according to the SNR for decreasing number of projections at 200° (decrease number of projections, upper graph) and decreasing angular range from 200° to 140° (decrease angular range, bottom graph). Circles correspond to SART-TV and squares to FDK. The SNR for the reference image (360° rotation, 720 projections, 15 mA and FDK.

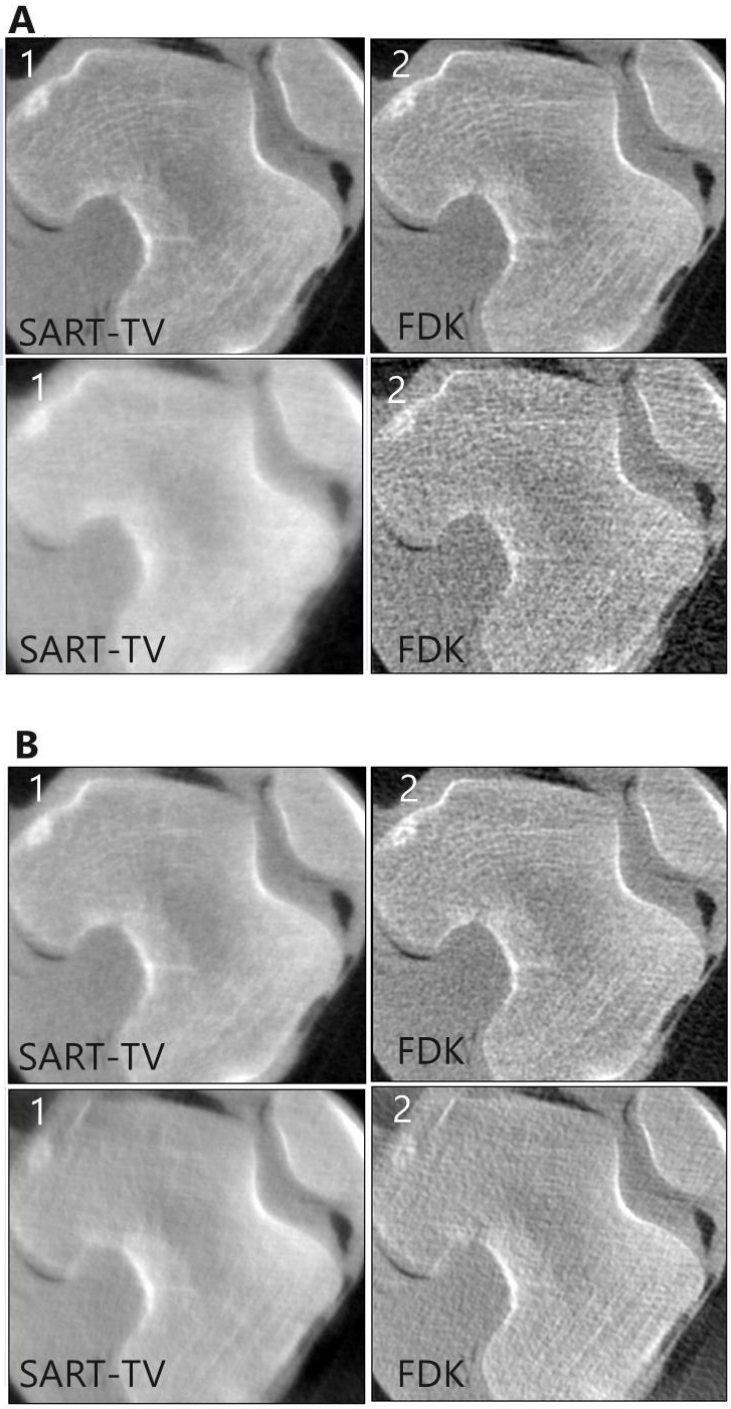

Figure 8: Image quality of the two reconstruction methods (Feldkamp-Davis-Kress [FDK] and simultaneous algebraic reconstruction technique [SART]) with a fixed angular range, 200°, and decrease in projection number- 400 projections (A1) and 80 projections (A2)- and decrease in angular range- 200° with 200 projections (B1) and 140° with 140 projections (B2).

4. Discussion

Real-time intra-operative imaging must be improved for unequivocal localization, identification of anatomical landmarks, and reinforcing the patient-specific anatomy knowledge. 3D CT reconstruction is ideal for guidance in interventional or orthopaedic fixation procedures because the results can be checked instantly and potentially corrected before leaving the operating room. All these factors help greatly enhance surgical confidence and could improve the learning curve for young orthopaedic surgeons [28]. Moreover, it could decrease the surgery time and radiation dose exposure to the patient and staff by avoiding unnecessary trial and error imaging. With orthopaedic surgery, one must be able to distinguish bone from soft tissue and restore the geometry of bone contours as much as possible. CB-CT imaging is based on a 2D flat panel detector and a cone-beam X-ray which yield isotropic voxel and high image spatial resolution [11]. Nevertheless, as compared with multidetector CT, the contrast resolution of the flat panel detector is lower because of lack of filtration and scatter rejection [14]. The important scatter radiation due to wider x-ray beam collimation in CB-CT leads to significant degradation of image quality as compared with classical CT. Combining CB-CT with a C-arm might have a negative effect on image quality and poses a great challenge to image reconstruction due to a limited angular span and possible artifacts when using conventional reconstruction methods. The FDK reconstruction method is classically used on CB-CT machine but iterative reconstruction (IR) can be used as an alternative method and has the ability to reduce image noise despite a significant reduction in tube current resulting in a reduction in overall radiation dose [15]. The aim of this study was to identify the acceptable limits in terms of number of projections with CB-CT, with a direct impact on dose radiation, for a preserved and interpretable image quality for orthopaedic applications. We simulated dose reduction by current reduction and/or by undersampling the projections and tested the classical algebraic reconstruction (SART-TV) as an iterative method of reconstruction compared to the FDK reconstruction with 720 projections over 360° at 15 mA. Thus, from our findings, SART-TV reconstruction is a good candidate for surgical orthopaedic applications, with a minimum of 200 projections. Objective indicators such as SNR, SSIM and DICE indexes derived from our segmentation analysis showed better results with SART-TV than FDK reconstruction in situations of low projection number and the reduction of rotation angular range. However, qualitative assessment and quality indexes derived on a grey level, such as RMSE and textural analysis, produced the best results with FDK reconstruction. The objective indicator SNR was relatively stable around 40 for SART-TV with decreased number of projections. In contrast, with FDK, the SNR decreased regularly with number of projections. The number of projections seemed to have more effects than reduction in angular span. Usually, all strategies for reducing radiation dose result in an increased image noise compromising diagnostic image quality [29]. Our results are consistent with classical CT iterative reconstruction: in a phantom of lumbar spine, Gervaise et al. found that adaptative iterative dose reduction reduced image noise without altering the spatial resolution as compared with filtered-back projection (FBP) [30]. In case of sparse acquisitions from 100 to 20 projections based on phantoms imaging, the contrast to noise ratio used for testing the similarity between the reconstructed and the FDK reference images have shown better results in case of iterative reconstruction compared to classical FDK

[21]. The use of IR in clinical CT of the spine allowed for 50% reduction of tube current intensity [31]. Indeed, the FBP and derived FDK reconstructions gave more details inside the bone volume (Figure 8) and were thus more frequently qualified as good by evaluators. One of the strengths of FBP reconstruction is well-known image texture [32]. The over-smooth appearance of IR reconstruction could affect the qualitative assessment because evaluators were not familiar with this appearance, contrary to FBP reconstruction. This observation was previously noted; IR methods are subject to over-smoothing degrading depiction of fine structure details and especially when the acquisition is at very low dose [17,32]. The RMSE is the simplest and widely used image-quality index, calculated by the root mean squared intensity differences of distorted and reference image pixels [33]. It is based on grey-level differences and details of the image: a well-textured image gives the best RMSE, which could explain the concordance we found with qualitative assessment. Most evaluators considered the FDK reconstructed images to have quite good quality as compared with SART-TV images. RMSE values were convergent with the qualitative assessment as was entropy, which is based on the co-occurrence matrix and an indicator of the coarseness aspect of texture. The structural similarity index (SSIM) is sensitive to the edge information between the reference and tested images and is considered reliable to assess structural information and structural distortion [33]. The similarity between the reconstructed and the FDK reference images have shown better results in case of iterative reconstruction compared to classical FDK [21]. On MRI images, the SSIM did not show significant correlation with the radiologist's opinion of diagnostic image quality, contrary to the RMSE [34]. Our results showed that for both RMSE and SSIM, reducing the number of projections beyond 200 is not recommended. Segmentation processes are considered of great importance in medical imaging, and segmentation quality is classically assessed by the DICE index [35]. The metric is sensitive to both the delineation of the boundary (contour) and the size (volume of the segmented object). In a previous study, we used 15 control points for initialization, followed by a snake model to segment joint space in knees [22]. Better results were clearly obtained with the IR reconstruction, with consistent results whatever the intensity, contrary to FDK. Therefore, The DICE index results are convergent with the SSIM results. One of the limitations of the study is to assess only one knee specimen but we are confident in the performance results as they can only be related to the different reconstruction scenarios everything else being equal. In the present study, we assessed only 3D reconstruction algorithms coupled with cone-beam acquisition. The geometrical deformation usually encountered with the C-arm, real-time tracking of the trajectory and calibration process have not been addressed. One other advantage of IR reconstruction is that it can integrate particular acquisition geometries that are potentially useful with a robotic C-arm capable of rotational orbits with oblique angulation [36]. Moreover, photon starvation artifacts, beam hardening, and metal artifacts likely decrease the quality of images. Further studies are required to study the impact of metal implants on IR reconstructions [37]. Nevertheless, TV regularization-based optimization integrated in the iterative framework has a positive effect for reducing metal artifacts [38]. As summary, the preservation of edges and geometry and the SNR were found favorable with an algebraic reconstruction even with low-dose protocol, with as a condition a minimum of 200 projections. The aim is not to restore

all details, contrasts and textures but to have an image quality sufficient with a good anatomical restoration of bone geometry. Consequently, image quality provided by algebraic reconstruction is probably sufficient with respect to high contrast anatomy for application in orthopaedic surgery.

Acknowledgements

We acknowledge the financial support of the program FUI-3Dc4arm.

Competing interests

Two of the authors of this manuscript (Guillaume Bernard and Fanny Morin) are employees of Thales AVS. The remaining authors declare that they have no competing interests.

References

1. Ning R, Chen B, Yu R, et al. Flat panel detector-based cone-beam volume CT angiography imaging: system evaluation. IEEE Trans Med Imaging 19 (2000): 949-963.
2. Siewerdsen JH, Moseley DJ, Burch S, et al. Volume CT with a flat-panel detector on a mobile, isocentric C-arm: pre-clinical investigation in guidance of minimally invasive surgery. Med Phys 32 (2005): 241-254
3. Gupta R, Grasruck M, Suess C, et al. Ultra-high resolution flat-panel volume CT: fundamental principles, design architecture, and system characterization. Eur Radiol 16 (2006): 1191-1205.
4. Feldkamp LA, Davis LC, Kress JW. Practical cone-beam algorithm J Opt Soc Am 1 (1984): 612-619
5. Pohlenz P, Blessmann M, Blake F, et al. Clinical indications and perspectives for intraoperative cone-beam computed tomography in oral and maxillofacial surgery. Oral Surg Oral Med Oral Pathol Oral Radiol Endod 103 (2007): 412-417.
6. Schouten R, Lee R, Boyd M, et al. Intra-operative cone-beam CT (O-arm) and stereotactic navigation in acute spinal trauma surgery. J Clin Neurosci 19 (2012): 1137-1143.
7. Tabaraee E, Gibson AG, Karahalios DG, et al. Intraoperative cone beam-computed tomography with navigation (O-ARM) versus conventional fluoroscopy (C-ARM): a cadaveric study comparing accuracy, efficiency, and safety for spinal instrumentation. Spine (Phila Pa 1976) 38 (2013): 1953-1958.
8. Khoury A, Whyne CM, Daly M, et al. Intraoperative cone-beam CT for correction of periaxial malrotation of the femoral shaft: a surface-matching approach. Med Phys 34 (2007): 1380-1387.
9. Khoury A, Siewerdsen JH, Whyne CM, et al. Intraoperative cone-beam CT for image-guided tibial plateau fracture reduction. Comput Aided Surg 12 (2007): 195-207.
10. Fahrig R, Dixon R, Payne T, et al. Dose and image quality for a cone-beam C-arm CT system. Med Phys 33 (2006): 4541-4550.
11. Akpek S, Brunner T, Benndorf G, et al. Three-dimensional imaging and cone beam volume CT in C-arm angiography with flat panel detector. Diagn Interv Radiol 11 (2005): 10-13.
12. Chau AC, Fung K. Comparison of radiation

dose for implant imaging using conventional spiral tomography, computed tomography, and cone-beam computed tomography. Oral Surg Oral Med Oral Pathol Oral Radiol Endod 107 (2009): 559-565.

13. Amiri S, Wilson DR, Masri BA, et al. A low-cost tracked C-arm (TC-arm) upgrade system for versatile quantitative intraoperative imaging. Int J Comput Assist Radiol Surg 9 (2014): 695-711.
14. Orth RC, Wallace MJ, Kuo MD, et al. C-arm Cone-beam CT: General Principles and Technical Considerations for Use in Interventional Radiology. Journal of Vascular and Interventional Radiology 19 (2008): 814-820.
15. Kalender WA. Dose in x-ray computed tomography. Phys Med Biol 59 (2014): 129-150.
16. Singh S, Kalra MK, Gilman MD, et al. Adaptive statistical iterative reconstruction technique for radiation dose reduction in chest CT: a pilot study. Radiology 259 (2011): 565-573.
17. Alshamari M, Geijer, Norrman E, et al. Low-dose computed tomography of the lumbar spine: a phantom study on imaging parameters and image quality. Acta Radiol 55 (2014): 824-832.
18. Gordon R, Bender R, and Herman GT. Algebraic reconstruction techniques (ART) for three-dimensional electron microscopy and X-ray photography. J Theor Biol 29 (1970): 471-481.
19. Kak AC, Slaney M. Principles of Computerized Tomographic Imaging (1988).
20. Andersen AH, Kak AC. Simultaneous algebraic reconstruction technique (SART): a superior implementation of the art algorithm. Ultrason Imaging 6 (1984): 81-94
21. Bian J, Siewerdsen JH, Han X, et al. Evaluation of sparse-view reconstruction from flat-panel-detector cone-beam CT. Phys Med Biol 12 (2010): 216575-216599.
22. Mezlini-Gharsallah H, Youssef R, Uk S, et al. Three-dimensional mapping of the joint space for the diagnosis of knee osteoarthritis based on high resolution computed tomography: Comparison with radiographic, outerbridge, and meniscal classifications. J Orthop Res 36 (2018): 2380-2391.
23. Lui Z, Laganière R. Phase congruence measurement for image similarity assessement. Pattern Recognition Letters 12 (2005): 166-172.
24. Gonzalez RC, Woods RE. Digital image processing, (3rd edtn), Prentice Hall, (2008), Upper Saddle River, N.J. USA.
25. Renieblas GP, Nogués AT, González AM, et al. Structural similarity index family for image quality assessment in radiological images. J Med Imaging (Bellingham) 4 (2017): 035501
26. Pedersen, M. Full-Reference Image Quality Metrics: Classification and Evaluation. FNT in Computer Graphics and Vision 7 (2011): 1-80.
27. Zijdenbos AP, Dawant BM, Margolin RA, and Palmer AC. Morphometric analysis of white matter lesions in MR images: Method and validation. IEEE Trans. Med. Imaging 13 (1994): 716-724.
28. Conlan TK, Beebe MJ, Weinlein JC. New Imaging, Diagnostic, and Assessment

Techniques in Orthopedic Trauma. Orthop Clin North Am 50 (2019): 47-56.

29. Willemink MJ, Leiner T, De Jong PA, et al. Iterative reconstruction techniques for computed tomography part 2: initial results in dose reduction and image quality. Eur Radiol 23 (2013): 1632-1642.
30. Gervaise A, Osemont B, Lecocq S, et al. CT image quality improvement using Adaptive Iterative Dose Reduction with wide-volume acquisition on 320-detector CT. Eur Radiol 22 (2012): 295-301.
31. Yang CH, Wu TH, Chiou YY, et al. Imaging quality and diagnostic reliability of low-dose computed tomography lumbar spine for evaluating patients with spinal disorders. Spine J 14 (2014): 2682-2690.
32. Stiller W. Basics of iterative reconstruction methods in computed tomography: A vendor-independent overview. Eur J Radiol 109 (2018): 147-154.
33. Wang Z, Bovik AC, Sheikh HR, et al. Image quality assessment: from error visibility to structural similarity. IEEE Trans Image Process 13 (2004): 600-612.
34. Mason A, Rioux J, Clarke SE, et al. Comparison of Objective Image Quality Metrics to Expert Radiologists' Scoring of Diagnostic Quality of MR Images. IEEE Trans Med Imaging 12 (2019): 19-26.
35. Taha AA, Hanbury A. Metrics for evaluating 3D medical image segmentation: analysis, selection, and tool. BMC Med Imaging 12 (2015): 15-29.
36. Stayman W and Siewerdsen J. Task-based trajectories in iteratively re-constructed interventional cone-beam CT. in Proceedings of the 12thMeeting on Fully Three-Dimensional Imaging Reconstruction in Radiology and Nuclear Medicine 11 (2013): 257-260.
37. Gang GJ, Stayman JW, Zbijewski W, et al. Task-based detectability in CT image reconstruction by filtered backprojection and penalized likelihood estimation. Medical Physics 41 (2014): 081902.
38. Zhang H. Iterative metal artifact reduction for x-ray computed tomography using unmatched projector/backprojector pairs. Medical Physics 43 (2016): 3019-3033.